Response Surface Model Based Emission Source Contribution and Meteorological Pattern Analysis in Ozone Polluted Days

Ying Chen[a], Yun Zhu[a, b, *], Chen-Jen Lin[c], Sarav Arunachalam[d], Shuxiao Wang[e], Jia Xing[e], Duohong Chen[f], Shaojia Fan[b], Tingting Fang[a], Anqi Jiang[a]

[a] Guangdong Provincial Key Laboratory of Atmospheric Environment and Pollution Control, College of Environment and Energy, South China University of Technology, Guangzhou Higher Education Mega Center, Guangzhou 510006, China

[b] Southern Marine Science and Engineering Guangdong Laboratory (Zhuhai), Sun Yat-Sen University, Zhuhai 519000, China

[c] Department of Civil and Environmental Engineering, Lamar University, Beaumont, TX, 77710, USA

[d] Institute for the Environment/CEMPD, The University of North Carolina at Chapel Hill, 100 Europa Drive, Chapel Hill, NC 27517, USA

[e] State Key Joint Laboratory of Environment Simulation and Pollution Control, School of Environment, Tsinghua University, Beijing 100084, China

[f] Guangdong Environmental Monitoring Center, Guangzhou 510308, China

* Correspondence to: Yun Zhu (zhuyun@scut.edu.cn)

ABSTRACT

Urban and regional ozone (O_3) pollution is a public health concern and causes damage to ecosystems. Due to the diverse emission sources of O_3 precursor and the complex interactions of air dispersion and chemistry, identifying the contributing sources for O_3 pollution requires integrated analysis for guiding emission reduction plans. In this study, the meteorological characteristics leading to O_3 polluted days (in which the O_3 levels are higher than the defined standard) in Guangzhou (GZ, China) were analyzed using the 2019 data. The O_3 formation regimes, source apportionments under various prevailing wind directions were evaluated using a Response Surface Modeling (RSM) approach. The results show that O_3 polluted days in GZ 2019 can be classified into four types of synoptic patterns (i.e., cyclone, anticyclone, trough, and high pressure approaching to sea) and are strongly correlated with high ambient temperature, low relative humidity, week wind speed, variable wind directions. Additionally, the cyclone pattern strongly promotes O_3 formation due to its peripheral subsidence. The O_3 formation is NO_x-limited under the northerly wind while VOC-limited under other prevailing wind directions in GZ. Anthropogenic emissions contribute largely to the O_3 formation of GZ (54-78%) under the westerly, southwesterly, easterly, southeasterly, or southerly wind, but only moderately (35-47%) under the northerly or northeasterly wind. Furthermore, local emissions have the largest O_3 contributions (39-60%) regardless of prevailing wind directions, especially the local NO_x contributions (19-43%). The dominant upwind regional emissions contributed to 12-46% of the O_3 formation in GZ (e.g., DG contributions are 12-20% under the southeasterly wind). The emission control strategies for O_3 polluted days should focus on local emission sources in conjunction with the emission reduction of upwind regional sources.

Keywords: O_3 pollution, Emission source contribution, Response Surface Model, Meteorology

1 Introduction

Over the past five years, the particulate matter ($PM_{2.5}$) levels have been reduced by 34% in the city cluster of the Pearl River Delta Region (PRD) in China, while the ambient ozone (O_3) concentrations have shown an upward trend. This air quality transition points O_3 as the primary pollutant in the region from 41% in 2015 to 67% in 2020 (DEEGP, 2021). In China, O_3 polluted days are those that have the maximum daily 8-h average (MDA8) O_3 concentration higher than the China Class II National O_3 Standard (160μg/m^3) and will cause serious damage to ecosystems. To lower the MDA8 O_3 concentrations, enhanced emission control during O_3 polluted days has been consistently requested by decision-makers in recent years. However, due to the complexity of O_3 formation in ambient air and the diverse source contribution of O_3 precursors, there is still a knowledge gap to formulate emission control policies for O_3 control in the region (Stevenson et al., 2013; Wang et al., 2009).

Earlier studies have apportioned the contributing emission sources leading to ambient O_3 pollution using the tagged tracer techniques in Air Quality Models (AQMs) (Ge et al., 2021; Li et al., 2013; Li et al., 2012; Shu et al., 2020). These works mostly focused on specific O_3 seasons and therefore did not adequately reveal the source contribution characteristics in relatively short periods of O_3 pollution. Besides, the tagged tracer techniques have limitations in representing the nonlinear relationship among O_3 and its precursors, especially NO_x (Chatani et al., 2020). Our recent developments of Response Surface Models (RSMs) has been demonstrated for their capability to quickly estimate the nonlinear response of O_3 to its precursors for emission source contribution analysis (Fang et al., 2020; Kelly et al., 2021; Xing et al., 2018; Xing et al., 2020; You et al., 2017). For instance, Xing et al. (2020) employed the RSM technique to identify the O_3 formation regime and indicated that NO_x emission reductions will increase the O_3 concentrations in the North China Plain under VOC-limited conditions. Fang et al. (2020) used the polynomial functions-based extended RSM technique integrated with differential methods (pf-ERSM-DM) to analyze the dynamic O_3 source contributions over the PRD and projected that the enhanced NO_x control can effectively lower the ambient O_3. However, these studies were also conducted in specific O_3 seasons which did not sufficiently incorporate analyses on the characteristics of meteorological patterns for elucidating the effects of prevailing wind directions that influence O_3 source apportionment results and account for the effect of upwind regional emissions and long-range transport (Berezina et al., 2020; Shao et al., 2009; Suthawaree et al., 2008).

Accordingly, taking Guangzhou (GZ, a representative megacity in the PRD) as an example, this study aims to advance the understanding of regional O_3 pollution through analyzing the meteorological characteristics leading to O_3 polluted days in GZ based on the 2019 data, then using the advanced Response Surface Modeling approach to identify the O_3 formation regimes, source apportionments under various prevailing wind directions. The analysis method and results are expected to assist decision-makers to formulate sound emission control strategies for O_3 polluted days and improve the O_3 attainment rate.

2 Methodology

The process of this study is shown in Fig. 1. Firstly, the O_3 polluted days of GZ 2019 are selected based on the monitoring data and the corresponding historical meteorological data (i.e., weather chart, temperature, relative humidity, wind speed, and prevailing wind direction) are also collected. Then the synoptic patterns in O_3 polluted days are classified by the weather charts and the corresponding meteorological characteristics under each synoptic pattern are analyzed. Secondly, the O_3 polluted days are divided into several O_3 episodes with various prevailing wind directions, and the control matrix for these O_3 episodes is designed based on the selected control factors (i.e., pollutants, regions) and parameterized by the 2019 PRD emission inventory (EI) to obtain scenario runs (Xing et al., 2011). Thirdly, the Community Multi-scale Air Quality model (CMAQ) simulations under various scenarios are driven by the 2019 PRD meteorology in O_3 episodes derived from the Weather Research and Forecast model (WRF), thereafter the simulation results are utilized to build the pf-ERSM-DM system. Finally, the O_3 formation regime is analyzed and the O_3 source apportionment is evaluated for identifying the major emission source contributors of O_3 under multi wind directions, regions, and precursors based on the established pf-ERSM-DM system (Fang et al., 2020).

2.1 Observation data source

The MDA8 O_3 concentrations of GZ are calculated by the average of that in the ten local national-controlled air-monitoring sites, and the locations of these sites are shown in Fig S1. In 2019, GZ suffered apparent O_3 pollution with the yearly 90th percentile of the MDA8 O_3 concentration reaching the peak over the past five years (Fig. S2), and a total of 54 O_3 polluted days happened as listed in Table S1 (the monitoring data are accessed in Guangdong Environmental Quality platform: http://113.108.142.147:20061/StationStatus/AppCheck). Accordingly, for analyzing meteorological patterns and emission source contributions in O_3 polluted days of GZ, the 2019 data was selected in this study.

The weather charts which are utilized to classify the synoptic patterns of O_3 polluted days in GZ 2019 are obtained from the Hong Kong Observatory (http://www.weather.gov.hk/tc/wxinfo/currwx/wxcht.htm). The main synoptic patterns of those polluted days can be divided into four types, namely cyclone, anticyclone, trough, and high pressure approaching to sea according to the classifications of the former researches (Huang et al., 2005; Pan et al., 2017). The typical examples of weather charts on each synoptic pattern are shown in Fig. S3. Meanwhile, the meteorological factors of O_3 polluted days in GZ 2019 including temperature, relative humidity, wind speed, and prevailing wind direction that can significantly affect the ambient O_3 (Han et al., 2020; Shao et al., 2009; Shi et al., 2020; Wang et al., 2017) are also collected. These meteorological data are acquired from the National Climate Data Center (https://www.ncei.noaa.gov/).

2.2 WRF-CMAQ simulation system

The O_3 episodes with various prevailing wind directions are listed in Table S2 which are selected based on the polluted days. The WRF version 3.9.1 is applied for providing the 2019 PRD meteorological inputs in the O_3 episodes for the CMAQ model and the CMAQ version 5.2 is utilized to simulate the O_3 concentration. Three nested domains (i.e., d01, d02, d03) used for the WRF-CMAQ model are shown in Fig. 2 and the horizontal resolutions of the three domains are 27km, 9km, 3km with the grid cells of 175×124, 133 × 133, 127 × 160 respectively. The innermost domain (d03) covering the entire PRD is divided into 8 regions, namely Guangzhou (GZ), Foshan (FS), Zhongshan (ZS), Jiangmen (JM), Dongguan (DG), Shenzhen (SZ), Huizhou (HZ) and the other regions in the d03 domain (OTH). For the d01 and d02 domains, the emission inventories offered by Tsinghua University are adopted (Multi-resolution Emission Inventory For China, MEIC: http://meicmodel.org). The 2019 PRD emission inventory of the d03 domain (Table S3) is developed by our research group. The Model of Emissions of Gases and Aerosols from Nature (Megan) version 2.10 (Guenther et al.,

2012) is utilized to prepare the natural emissions. The initial and boundary files of the d02 and d03 domain are from the CMAQ simulation results on the upper domain and a 5-day spin-up time is used to rid of the initial condition influence. The detailed parameter configurations for WRF and CMAQ are shown in Table S4 and Table S5. The performance of WRF and CMAQ is detailed in section 3 of Supporting Information (SI).

2.3 Response surface modeling technology

RSM is a meta-model established from the CMAQ simulation results with the ability to quickly and accurately estimate the pollutant response to emission source perturbations. The pf-ERSM-DM system is used in this study, which has been elaborated on in our latest paper (Fang et al., 2020; 2021). The experiment design for constructing pf-ERSM-DM is presented in Table S6 and the matching control matrix is the same for each O_3 episode as shown in Fig. S4. Summarily, there are 181 scenario runs of CMAQ simulations sampled by the Hamersley quasi-random Sequence Sampling (HSS) with the emission ratio ranges from 0.0 to 1.5, including one baseline scenario (=1.0), 8 single regional RSMs (for the d03 domain being divided into 8 regions), and one multiple regional RSM. For a single regional RSM, 20 scenarios are established for the response of O_3 in the individual receptor region to precursor emission changes in the individual source region, and emissions from the other source regions are consistent with the baseline. For multiple regional RSM, 20 scenarios are created for O_3 response in individual receptor regions to simultaneous precursor emission changes from all source regions. Additionally, 10 extra scenarios which are also sampled by HHS are used for out-of-sample (OOS) validation to evaluate the accuracy of the established pf-ERSM-DM system, and the OOS validation results are detailed in section 3 of SI.

3 Results and discussion

3.1 Meteorological characteristics under various synoptic patterns in O_3 polluted days

To analyze the meteorological patterns associated with O_3 polluted days in GZ 2019, four main synoptic patterns and their corresponding meteorological characteristics are summarized in Table 1.

The cyclone pattern has the highest occurrence frequency of 26 days, mainly happening in summer and autumn. Under this pattern, it exhibits a high temperature (mean value is 31℃) and a dry air layer (mean relative humidity is 52%) in the low troposphere which are affected by the thermal effects-driven from the strong subsidence airflow at the outskirts of this pattern, causing the average value of MDA8 O_3 concentration (200μg/m^3, with the range of 165-248μg/m^3) significantly higher than that under the other three synoptic patterns. The anticyclone pattern occurred in spring, summer, and autumn, with the frequency of 14 days, in which the accumulation of pollutants is promoted at the periphery of this pattern. Compared with the other three patterns, the mean temperature (27℃, with the range of 17-34℃) is relatively low and the mean wind speed (1.32m/s) is at a comparatively high level which may cause the average value of MDA8 O_3 concentration (187μg/m^3, with a range of 163-228μg/m^3) of this pattern is the lowest. The trough is situated in the vicinity of the east over the South China Sea happening for 9 days in autumn, under which the average value of MDA8 O_3 concentration (190μg/m^3) is ranked third among the four synoptic patterns. The mean wind speed is relatively weak (1.25m/s), while the mean relative humidity (54%, with the range of 30-80%) is higher than that under the other synoptic patterns. The high pressure approaching to sea pattern occurred the least days of 5 in spring and autumn. Under this circumstance, GZ is located at the bottom of the high-pressure ridge, in which the mean wind speed (1.08m/s, with a range of 0.3-2.4m/s) is the lowest among the four synoptic patterns, and the average value of MDA8 O_3 concentration (192μg/m^3) under this pattern is the second-highest.

Moreover, it is noticed that the prevailing wind directions under all synoptic patterns are generally variable. Due to the fact that GZ is located in the center of the PRD surrounded by abundant emission sources, the wind blowing from any direction may bring the transmission of pollutants to the local and influence its O_3 formation. Hence, further analysis of emission source contribution in O_3 polluted days of GZ under various prevailing wind directions is needed and detailed in the following sections.

3.2 Analysis of O_3 formation regime

The 2-D isopleth of O_3 is plotted with the emission ratios of VOC and NO_x as the X and Y axes, and the combination emission ratios of VOC and NO_x that produce the same O_3 concentrations are connected through isolines (Li et al., 2022). This isopleth can provide useful information about the O_3 formation regime (i.e., VOC-limited or NO_x-limited regime) which reflects the nonlinearity between O_3 and its precursor emissions (Fang et al., 2020; Jin et al., 2021). In our previous research, the peak ratio (PR), which is described in Text S4, has been used as the indicator to determine the O_3 formation regime (Xing et al., 2018). In general, the PR value lower than 1 suggest that the O_3 formation is VOC-limited, otherwise, it is NO_x-limited. To analyze the O_3 formation regime in O_3 episodes of GZ 2019, the 2-D isopleths of O_3 response (The average value of MDA8 O_3 concentrations in O_3 episodes of GZ under various prevailing wind directions) in GZ to Anthropogenic VOC (AVOC) and NO_x emission changes from all source regions in the d03 domain are obtained and the corresponding PR values are also calculated, as shown in Fig. 3.

When the same wind prevails, the trend of 2-D isopleths is analogous and the PR values exhibit little difference with the range of 0-0.14. However, the PR value of O_3 episode in summer is higher than that in other seasons under the same prevailing wind, which is due to the seasonal variation of Biogenic VOC (BVOC) emissions while NO_x emissions vary slightly in different seasons (Fang et al., 2020; Shao et al., 2009; Yang et al., 2019). It can also be found that the average PR values under the northerly, westerly, northeasterly, southwesterly, easterly, southerly, southeasterly wind are 1.08, 0.80, 0.79, 0.69, 0.60, 0.48, 0.44 respectively. The average PR value is the highest under the northerly wind since the BVOC emissions are relatively plentiful in the north of GZ while the NO_x emissions are comparatively small as shown in Fig. S5, which may facilitate the O_3 formation in GZ to the NO_x-limited regime because of the dominant reaction of NO with peroxyl radicals. When the southeasterly wind prevails, the NO_x emissions in local and upwind cities are abundant, while the VOC emissions are relatively small. In this case, the main removal process of free radicals is their reaction with NO_2 to forms the nitric acid, hence the O_3 formation will be mainly determined by the generation rate of free radicals, resulting in the strong VOC-limited regime and the lowest average PR value.

Under the northerly wind, the O_3 formation in GZ is NO_x-limited ($1.03 < PR < 1.11$), indicating that the priority control of NO_x (even at slight reductions) will have a more obvious effect on O_3 mitigations while the influence of VOC reduction is comparably tiny. Under the other prevailing wind directions, the O_3 formation in GZ is generally VOC-limited ($0.38 < PR < 0.82$), implying that an initial VOC control is conducive to reducing the baseline O_3 levels in GZ, whereas the NO_x emission reductions will increase the O_3 concentration initially because of the competition between NO_2 and VOC for OH radicals. Only the NO_x emission reduction rate greater than 18-62% can make the O_3 formation regime be transferred to the NO_x-limited condition and lower the O_3 concentrations in GZ. Additionally, to prevent the phenomenon of NO_x emissions being reduced but the O_3 concentration is rising, the minimum VOC/NO_x reduction ratios (VNrs) are also calculated and described in Text S4 (Xing et al., 2018). Accordingly, the VNrs are 1.13-1.15, 1.20, 1.33, 1.33-1.53, 1.43-1.47, 1.45-1.87 under the westerly, northeasterly, southwesterly, easterly, southerly, southeasterly wind, respectively. The results show that the VNr is negatively correlated with the PR which indicates that a stronger VOC-limited regime requires more simultaneous VOC control with NO_x; besides, the VNrs fluctuate with the change of the prevailing wind directions, which needs to be considered in emission control policy formulation.

3.3 Analysis of O_3 source apportionments

3.3.1 Anthropogenic and background contributions to O_3

Differentiating of the anthropogenic contribution (anthropogenic emission sources of VOC and NO_x within the d03 domain) and background contribution (including initial condition, boundary condition, and the non-human controllable emission sources of VOC and NO_x) (You et al., 2017) to O_3 can offer information about the maximum achievable O_3 concentration targets and support for formulating effective O_3 control strategies. Through the established pf-ERSM-DM system, the anthropogenic and background contributions to O_3 in GZ (The average value of MDA8 O_3 concentrations in O_3 episodes of GZ under various prevailing wind directions) can be quantitatively analyzed when eliminating all anthropogenic emissions as shown in Fig. 4.

Under either the westerly or the easterly wind, the occurrences of O_3 polluted days are few with 5 days. The base O_3 concentrations under the westerly wind are relatively high with a range of 202-214 μg/m^3 while that under the easterly wind (162-176 μg/m^3) are comparatively low. Under these two prevailing wind directions, the anthropogenic emissions have large O_3 contributions accounting for 65-78%, and the base O_3 concentrations can be reduced to the greatest extent of 44-67μg/m^3. When the southeasterly wind prevails, the O_3 episodes occurred the most frequently and the base O_3 concentrations vary in a wide range of 165-219μg/m^3. In this condition, the anthropogenic contributions account for 54-63%, which are lower than that under the westerly or easterly wind, and the base O_3 concentrations can be reduced to 69-

90μg/m^3. These relatively low anthropogenic contributions under the southeasterly wind may be explained by the ocean inflow transported upstream. Similar to the situation under the southeasterly wind, the anthropogenic contributions under the southwesterly or southerly wind are 55-63%, and thus the base O_3 concentrations can be reduced from 170-203μg/m^3 to the background O_3 concentrations of 66-84μg/m^3. The northeast and north wind usually prevail in autumn, in which the base O_3 concentrations are also high with the range of 172-206μg/m^3, while the anthropogenic contributions are less than 50% overall. Under these two conditions, the O_3 concentrations of GZ are significantly influenced by the emissions transported from the continental regions of China, resulting in high background O_3 concentrations (104-120μg/m^3) which are above China Class I National O_3 Standard (100μg/m^3). Therefore, the implementation of stricter control policies on a larger spatial scale rather than only the PRD may be needed to further decrease the O_3 concentrations in GZ under the northeasterly or northerly wind.

Additionally, according to the previous O_3 source contribution analysis conducted in entire months fitted by the pf-ERSM-DM system, the anthropogenic contributions to the O_3 in GZ are 32% and 45% under northeasterly and southwesterly wind respectively (Fang et al., 2020). While, the anthropogenic contributions in O_3 episodes estimated in this study increase to 47% and 63% when the northeasterly and southwesterly wind prevail separately, the anthropogenic contributions matter a lot than that in entire months may be due to the relatively stagnant weather conditions in O_3 episodes.

3.3.2 Anthropogenic contributions to O_3 under multi wind directions, regions, and precursors

To determine the anthropogenic contributions to O_3 under multi wind directions, regions, and precursors, the total NO_x and VOC contributions from multiregional emission sources to the O_3 in GZ are calculated (Table S10). The NO_x and VOC emission contributions from each source region in the d03 domain to the O_3 in GZ under various prevailing wind directions are furtherly estimated, as shown in Fig. 5 and detailed in Table S11.

Considering the total contributions of multiregional NO_x and VOC emissions, it can be seen that NO_x makes more significant contributions (52-80%) than VOC under all prevailing wind directions except under the southeasterly wind in which the total NO_x contributions (46-48%) are slightly lower than the VOC in some O_3 episodes. Additionally, the total NO_x contributions under various prevailing wind directions show a declining trend as follows: north (73-80%), west (68-70%), northeast (66%), southwest (63%), east (55-58%), south (52-56%), southeast (46-55%), and this trend may be elucidated by the variation of the corresponding O_3 formation regimes. For example, the O_3 formation in GZ is typical NO_x-limited ($1.03 < PR < 1.11$) under the northerly wind when the depth NO_x emission reductions can significantly lower the O_3 concentrations, resulting in the largest total NO_x contributions.

GZ is an urban and prosperous city located in the central part of the PRD, with abundant O_3 precursor emissions, as for the contributions from each source region to the O_3 in GZ, the local contributions (39-60%) are always the highest regardless of prevailing wind directions. Furthermore, compared with the local contributions of an entire month (12-17%) in the former study evaluated by the pf-ERSM-DM system (Fang et al., 2020), the local contributions in O_3 episodes obviously increase more than 20% and these similar results have also been proved in other related researches (Li et al., 2012; Yang et al., 2019). This phenomenon may be explained by the conductive meteorological conditions in O_3 episodes which favor the chemical formation of O_3 and lead to considerably high local contributions. Additionally, the GZ-NO_x contributions (19-43%) are higher than GZ-VOC contributions (11-28%) in most O_3 episodes, this is because the O_3 formation in GZ will transit to NO_x-limited when strengthening the emission reductions, hence the influence of enhanced NO_x reduction on O_3 will be more obvious than that of VOC.

Apart from the local contributions, the major regional emission source contributors in different O_3 episodes are closely related to the prevailing wind direction. Under the northerly wind, the O_3 and its precursors may be transported from the northern PRD (i.e.g., Qingyuan) to GZ, thus, OTH-NO_x emissions show an obvious impact of 26-37% and OTH-VOC contributions are also great accounting for 7-12%. Similar to that under the northerly wind, OTH-NO_x contributions account for a large amount of 19% under the northeasterly wind. When the westerly wind prevails, FS-NO_x and FS-VOC contribute a substantial percentage of 13-17% and 7-10% respectively to the O_3 in GZ, because FS is an essential industrial/manufacture base and a comprehensive transportation hub in the PRD with intensive VOC and NO_x emissions; besides, OTH-NO_x contributions also account for a relatively large proportion of 10-15%. Under the southwesterly wind, FS-NO_x has a large O_3 contribution of 13%; OTH-NO_x also occupies a nonnegligible proportion of 11% which may mostly be from Zhaoqing (an important transportation hub that connects economically developed regions with southwestern provinces) and Zhuhai (a major coastal port of China). Under the southerly wind, FS also has a great impact, with FS-NO_x and FS-VOC contributions accounting for 10-13% and 7-8% respectively. DG is a city with relatively rapid urbanization in the PRD, containing large amounts of industrial factories and vehicles, thus under the southeasterly wind, DG-NO_x and DG-VOC contributions are great accounting for 5-11% and 6-11% respectively; OTH-NO_x also has an important impact of 5-10%, which may result from the intensive emissions in the coastal areas of OTH. Resemble the situations under the southeasterly wind, when the easterly wind prevails, DG-VOC and DG-NO_x contributions account for 8% and 6-7%, respectively; the contributions from OTH increase slightly, with OTH-NO_x contributions accounting for 7-8%.

4 Conclusions

In this study, the meteorological characteristics leading to O_3 polluted days in GZ were analyzed in a typical year (2019) with frequent O_3 episodes, and the O_3 formation regimes and source apportionments in O_3 episodes under various prevailing wind directions are comprehensively evaluated based on the pf-ERSM-DM system.

The ambient O_3 pollution is strongly related to meteorological patterns. The O_3 polluted days in GZ 2019 can be classified into four major synoptic patterns (i.e., cyclone, anticyclone, trough, and high pressure approaching to sea) and they generally exhibit similar meteorological characteristics favoring the chemical production of O_3 in GZ, including high mean temperature (26-31℃), low mean relative humidity (48-54%), weak mean wind speed (1.08-1.34m/s) and variable prevailing wind directions. Additionally, the cyclone pattern strongly promotes O_3 formation due to its peripheral subsidence.

From the perspective of emission control in O_3 polluted days, it is momentous to identify the O_3 formation regime and quantitatively comprehend the precursor emissions in shaping anthropogenic and background contributions. The O_3 formation regime and source apportionment results are highly related to the prevailing wind directions due to the abundant pollutants transported from the anthropogenic emission sources in the upwind areas. Under the westerly, southwesterly, easterly, southeasterly, or southerly wind, the O_3 formation in GZ is generally VOC-limited and the anthropogenic emissions have large O_3 contributions (54-78%); while under the northeasterly or northerly wind, the O_3 formation is weak VOC-limited and NO_x-limited respectively, and the anthropogenic contributions are relatively moderate (35-47%) resulting in comparatively high background O_3 concentrations which even exceed the China Class I National O_3 Standard (100μg/m^3). In terms of anthropogenic contributions, the local contributions account for the largest proportion (39-60%) regardless of prevailing wind directions, especially the GZ-NO_x which occupies a high contribution ratio (19-43%); upwind regional emission sources also had large O_3 contributions (12-46%).

Consequently, the sound emission control strategies for O_3 polluted days should be implemented with the consideration of prevailing wind direction. First, the NO_x control (even at slight reductions) should be strengthened under the northerly wind; while the short-term coordinated control of VOC and NO_x and long-term enhanced control of NO_x are suggested under the other prevailing wind directions. Second, the city-scale cooperation on anthropogenic emission reductions within the PRD should be enhanced under the westerly, southwesterly, easterly, southeasterly, or southerly wind; whereas the emission control on a larger spatial scale rather than only the PRD will be more effective under the northerly or northeasterly wind. Finally, the prior control of local precursor emissions in conjunction with flexible reinforcing upwind regional emission control based on prevailing wind direction is recommended to reduce the O_3 levels and improve the O_3 attainment rate in GZ.

Acknowledgments

This work was supported by the Science and Technology Program of Guangzhou, China (No. 202002030188), the Innovation Group Project of Southern Marine Science and Engineering Guangdong Laboratory (Zhuhai) (No. 311021001), the Science and Technology Planning Project of Guangdong Province, China (No. 2018208). The authors sincerely thank Dr. Carey Jang and (U.S. Environmental Protection Agency) for their assistance in the preparation and management of this paper. The views expressed in this paper are those of the authors alone and do not necessarily reflect the views and policies of the U.S. Environmental Protection Agency.

References

Berezina, E., Moiseenko, K., Skorokhod, A., Pankratova, N. V., Belikov, I., Belousov, V., Elansky, N. F. 2020. Impact of VOCs and NOx on Ozone Formation in Moscow. Atmos. 11(11). https://doi.org/10.3390/atmos11111262.

Chatani, S., Shimadera, H., Itahashi, S., Yamaji, K. 2020. Comprehensive analyses of source sensitivities and apportionments of PM2.5 and ozone over Japan via multiple numerical techniques. Atmos. Chem. Phys. 20(17), 10311-10329. https://doi.org/10.5194/acp-20-10311-2020.

DEEGP. 2021. 2020 Report on the state of Guangdong provincial ecology and environment. http://gdee.gd.gov.cn/hjzkgb/content/post_3266052.html, Accessed date: 19 April 2021 (in Chinese).

Fang, T., Zhu, Y., Jang, J., Wang, S., Xing, J., Chiang, P.-C., Fan, S., You, Z., Li, J. 2020. Real-time source contribution analysis of ambient ozone using an enhanced meta-modeling approach over the Pearl River Delta Region of China. J. Environ. Manag. 268. https://doi.org/10.1016/j.jenvman.2020.110650.

Fang, T., Zhu, Y., Wang, S., Xing, J., Zhao, B., Fan, S., Li, M., Yang, W., Chen, Y., Huang, R. 2021. Source impact and contribution analysis of ambient ozone using multi-modeling approaches over the Pearl River Delta region, China. Environ. Pollut. 289. https://doi.org/10.1016/j.envpol.2021.117860.

Ge, S., Wang, S., Xu, Q., Ho, T. 2021. CAMx simulations of the control of anthropogenic emissions on the reduction of ozone formation in Southeast Texas of USA. Atmos. Pollut. Res. 12(7). https://doi.org/10.1016/j.apr.2021.101114.

Guenther, A. B., Jiang, X., Heald, C. L., Sakulyanontvittaya, T., Duhl, T., Emmons, L. K., Wang, X. 2012. The Model of Emissions of Gases and Aerosols from Nature version 2.1 (MEGAN2.1): an extended and updated framework for modeling biogenic emissions. Geosci. Model Dev. (GMD) 5(6), 1471-1492. https://doi.org/10.5194/gmd-5-1471-2012.

Han, H., Liu, J., Shu, L., Wang, T., Yuan, H. 2020. Local and synoptic meteorological influences on daily variability in summertime surface ozone in eastern China. Atmos. Chem. Phys. 20(1), 203-222. https://doi.org/10.5194/acp-20-203-2020.

Huang, J. P., Fung, J. C. H., Lau, A. K. H., Qin, Y. 2005. Numerical simulation and process analysis of typhoon-related ozone episodes in Hong Kong. J. Geophys. Res. Atmos. 110(D5). https://doi.org/10.1029/2004jd004914.

Jin, J., Zhu, Y., Jang, J., Wang, S., Xing, J., Chiang, P.-C., Fan, S., Long, S. 2021. Enhancement of the polynomial functions response surface model for real-time analyzing ozone sensitivity. Front. Environ. Sci. Eng. 15(2). https://doi.org/10.1007/s11783-020-1323-0.

Kelly, J. T., Jang, C., Zhu, Y., Long, S., Xing, J., Wang, S., Murphy, B. N., Pye, H. O. T. 2021. Predicting the Nonlinear Response of PM2.5 and Ozone to Precursor Emission Changes with a Response Surface Model. Atmos. 12(8). https://doi.org/10.3390/atmos12081044.

Li, J., Dai, Y., Zhu, Y., Tang, X., Wang, S., Xing, J., Zhao, B., Fan, S., Long, S., Fang, T. 2022. Improvements of response surface modeling with self-adaptive machine learning method for PM2.5 and O-3 predictions. J. Environ. Manag. 303. https://doi.org/10.1016/j.jenvman.2021.114210.

Li, Y., Lau, A. K. H., Fung, J. C. H., Ma, H., Tse, Y. 2013. Systematic evaluation of ozone control policies using an Ozone Source Apportionment method. Atmos. Environ. 76, 136-146. https://doi.org/10.1016/j.atmosenv.2013.02.033.

Li, Y., Lau, A. K. H., Fung, J. C. H., Zheng, J. Y., Zhong, L. J., Louie, P. K. K. 2012. Ozone source apportionment (OSAT) to differentiate local regional and super-regional source contributions in the Pearl River Delta region, China. J. Geophys. Res. Atmos. 117. https://doi.org/10.1029/2011jd017340.

Pan, Y., Chen, D., Ye, S., Shen, J., Ji, P., Wang, Y., Xie, M., Xu, F. 2017. Characteristics and Influential Factors of Typical Air Pollution Events in Guangdong Province. Safety. Environ. Enginee. 24(02), 58-66. https://doi.org/10.13578/j.cnki.issn.1671-1556.2017.02.010, (in Chinese).

Shao, M., Zhang, Y., Zeng, L., Tang, X., Zhang, J., Zhong, L., Wang, B. 2009. Ground-level ozone in the Pearl River Delta and the roles of VOC and NOx in its production. J. Environ. Manag. 90(1), 512-518. https://doi.org/10.1016/j.jenvman.2007.12.008.

Shi, Z., Huang, L., Li, J., Ying, Q., Zhang, H., Hu, J. 2020. Sensitivity analysis of the surface ozone and fine particulate matter to meteorological parameters in China. Atmos. Chem. Phys. 20(21), 13455-13466. https://doi.org/10.5194/acp-20-13455-2020.

Shu, L., Wang, T., Han, H., Xie, M., Chen, P., Li, M., Wu, H. 2020. Summertime ozone pollution in the Yangtze River Delta of eastern China during 2013-2017: Synoptic impacts and source apportionment. Environ. Pollut. 257. https://doi.org/10.1016/j.envpol.2019.113631.

Stevenson, D. S., Young, P. J., Naik, V., Lamarque, J. F., Shindell, D. T., Voulgarakis, A., Skeie, R. B., Dalsoren, S. B., Myhre, G., Berntsen, T. K., Folberth, G. A., Rumbold, S. T., Collins, W. J., MacKenzie, I. A., Doherty, R. M., Zeng, G., van Noije, T. P. C., Strunk, A., Bergmann, D., Cameron-Smith, P., Plummer, D. A., Strode, S. A., Horowitz, L., Lee, Y. H., Szopa, S., Sudo, K., Nagashima, T., Josse, B., Cionni, I., Righi, M., Eyring, V., Conley, A., Bowman, K. W., Wild, O., Archibald, A. 2013. Tropospheric ozone changes, radiative forcing and attribution to emissions in the Atmospheric Chemistry and Climate Model Intercomparison Project (ACCMIP). Atmos. Chem. Phys. 13(6), 3063-3085. https://doi.org/10.5194/acp-13-3063-2013.

Suthawaree, J., Kato, S., Takami, A., Kadena, H., Toguchi, M., Yogi, K., Hatakeyama, S., Kajii, Y. 2008. Observation of ozone and carbon monoxide at Cape Hedo, Japan: Seasonal variation and influence of long-range transport. Atmos. Environ. 42(13), 2971-2981. https://doi.org/10.1016/j.atmosenv.2007.12.053.

Wang, T., Wei, X. L., Ding, A. J., Poon, C. N., Lam, K. S., Li, Y. S., Chan, L. Y., Anson, M. 2009. Increasing surface ozone concentrations in the background atmosphere of Southern China, 1994-2007. Atmos. Chem. Phys. 9(16), 6217-6227. https://doi.org/10.5194/acp-9-6217-2009.

Wang, T., Xue, L., Brimblecombe, P., Lam, Y. F., Li, L., Zhang, L. 2017. Ozone pollution in China: A review of concentrations, meteorological influences, chemical precursors, and effects. Sci. Total Environ. 575, 1582-1596. https://doi.org/10.1016/j.scitotenv.2016.10.081.

Xing, J., Ding, D., Wang, S., Zhao, B., Jang, C., Wu, W., Zhang, F., Zhu, Y., Hao, J. 2018. Quantification of the enhanced effectiveness of NOx control from simultaneous reductions of VOC and NH3 for reducing air pollution in the Beijing-Tianjin-Hebei region, China. Atmos. Chem. Phys. 18(11), 7799-7814. https://doi.org/10.5194/acp-18-7799-2018.

Xing, J., Li, S., Jiang, Y., Wang, S., Ding, D., Dong, Z., Zhu, Y., Hao, J. 2020. Quantifying the emission changes and associated air quality impacts during the COVID-19 pandemic on the North China Plain: a response modeling study. Atmos. Chem. Phys. 20(22), 14347-14359. https://doi.org/10.5194/acp-20-14347-2020.

Xing, J., Wang, S. X., Jang, C., Zhu, Y., Hao, J. M. 2011. Nonlinear response of ozone to precursor emission changes in China: a modeling study using response surface methodology. Atmos. Chem. Phys. 11(10), 5027-5044. https://doi.org/10.5194/acp-11-5027-2011.

Yang, W., Chen, H., Wang, W., Wu, J., Li, J., Wang, Z., Zheng, J., Chen, D. 2019. Modeling study of ozone source apportionment over the Pearl River Delta in 2015. Environ. Pollut. 253, 393-402. https://doi.org/10.1016/j.envpol.2019.06.091.

You, Z., Zhu, Y., Jang, C., Wang, S., Gao, J., Lin, C.-J., Li, M., Zhu, Z., Wei, H., Yang, W. 2017. Response surface modeling-based source contribution analysis and VOC emission control policy assessment in a typical ozone-polluted urban Shunde, China. J. Environ. Sci. 51, 294-304. https://doi.org/10.1016/j.jes.2016.05.034.

Figures and Tables

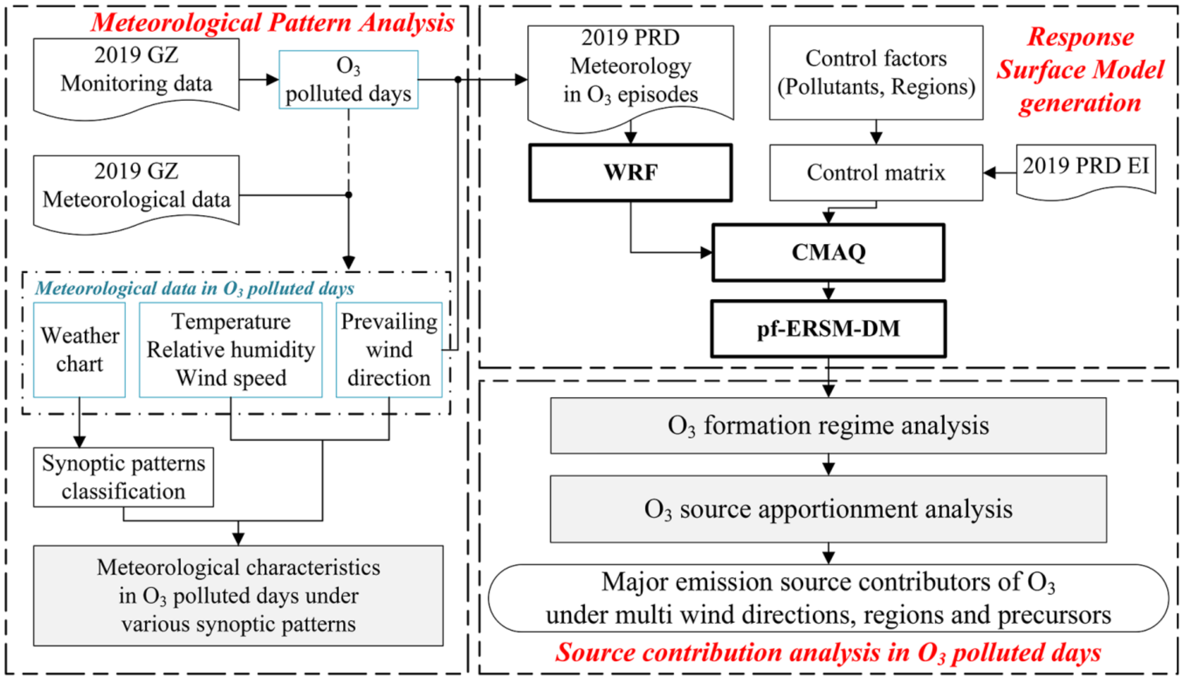

Fig. 1. The flow scheme for response surface model based emission source contribution and meteorological pattern analysis in ozone polluted days.

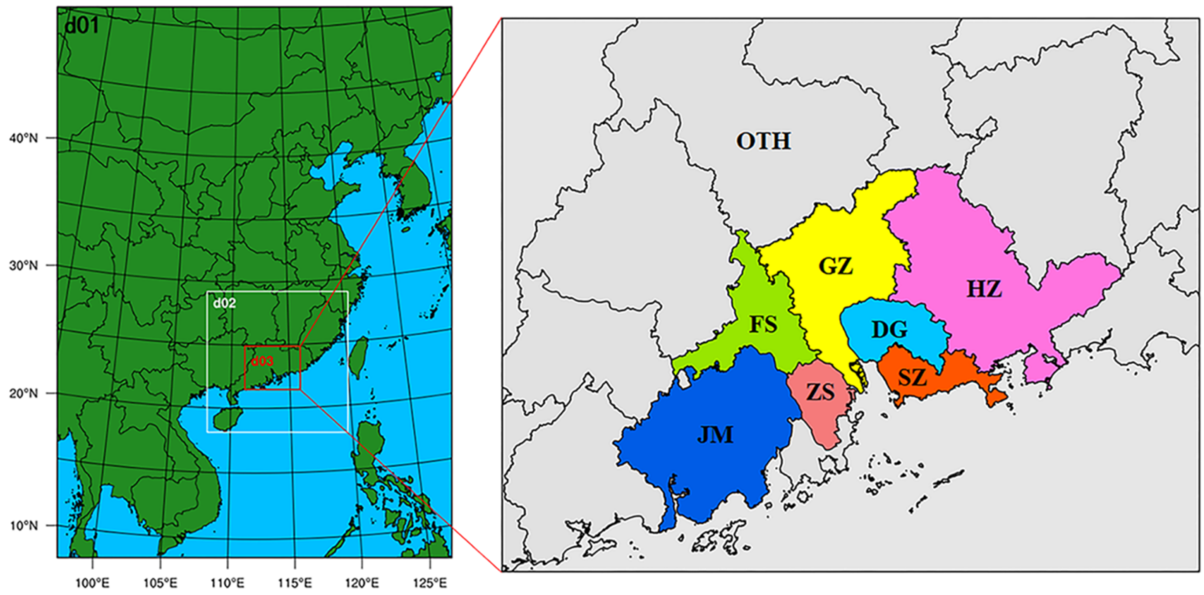

Fig. 2. Three simulation domains and the regions in the d03 domain. GZ - Guangzhou; FS - Foshan; ZS - Zhongshan; JM - Jiangmen; DG - Dongguan; SZ - Shenzhen; HZ – Huizhou; OTH – The other regions in the d03 domain.

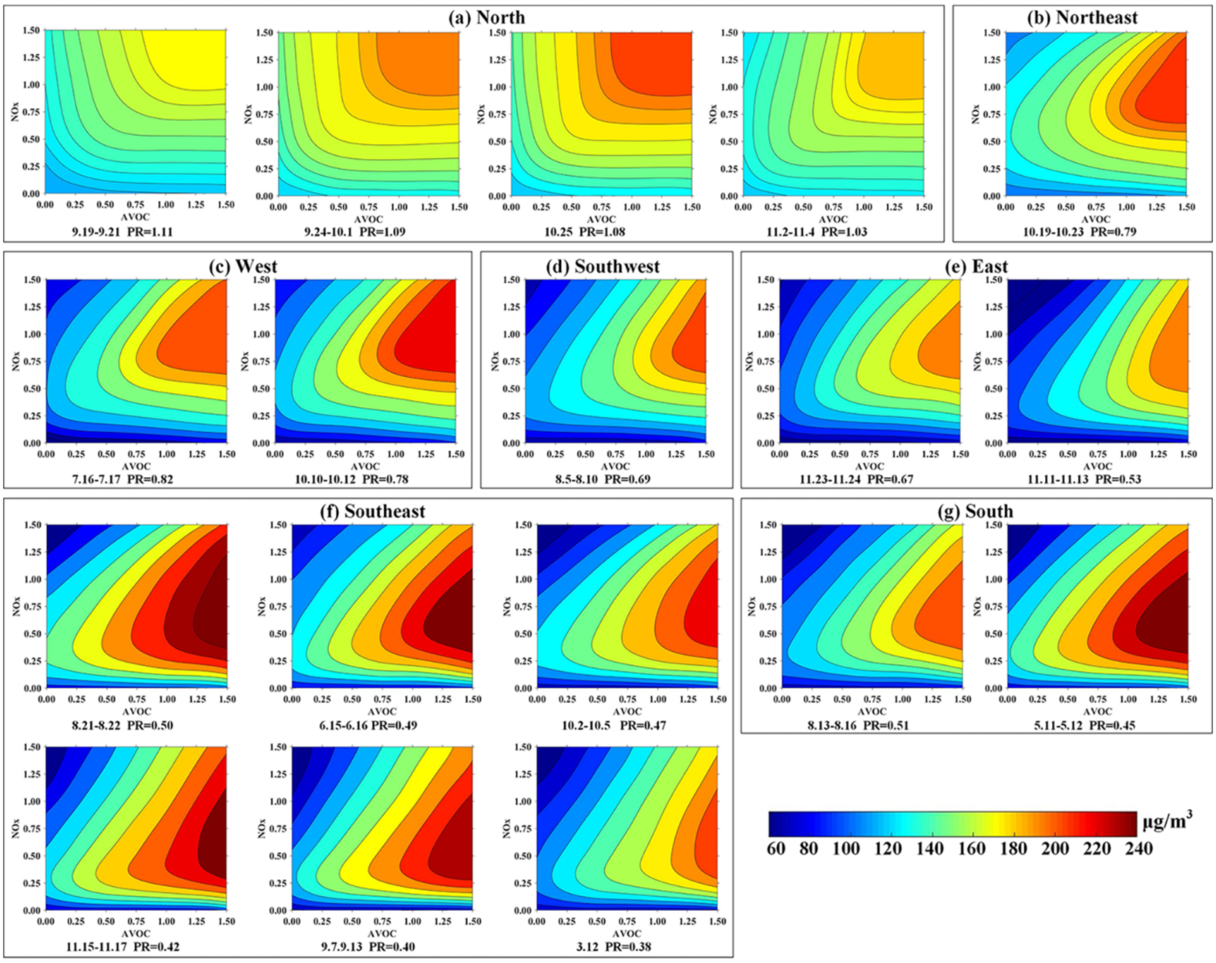

Fig. 3. The 2-D isopleths of O_3 response in GZ to AVOC and NO_x emission changes from all source regions in the d03 domain and their matching PR value. The X and Y-axes show the emission ratio of AVOC and NO_x for the entire d03 domain; Different O_3 concentrations are presented in different colors.

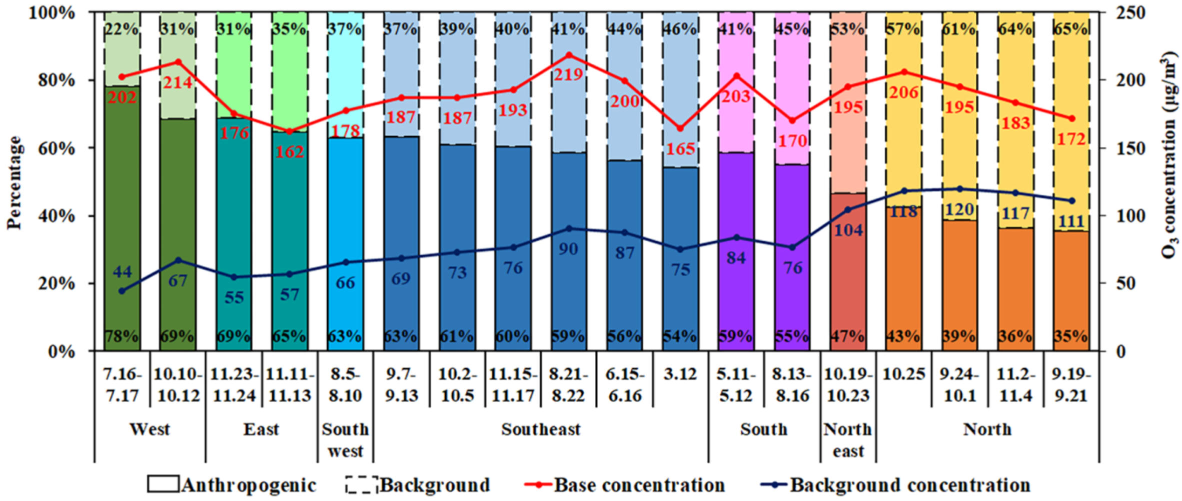

Fig. 4. Anthropogenic contribution within the d03 domain and the background contribution to O_3 concentrations in GZ. Base concentration: O_3 concentration under base scenario; Background concentration: O_3 concentration under background contribution; Different colors distinguish different prevailing wind directions.

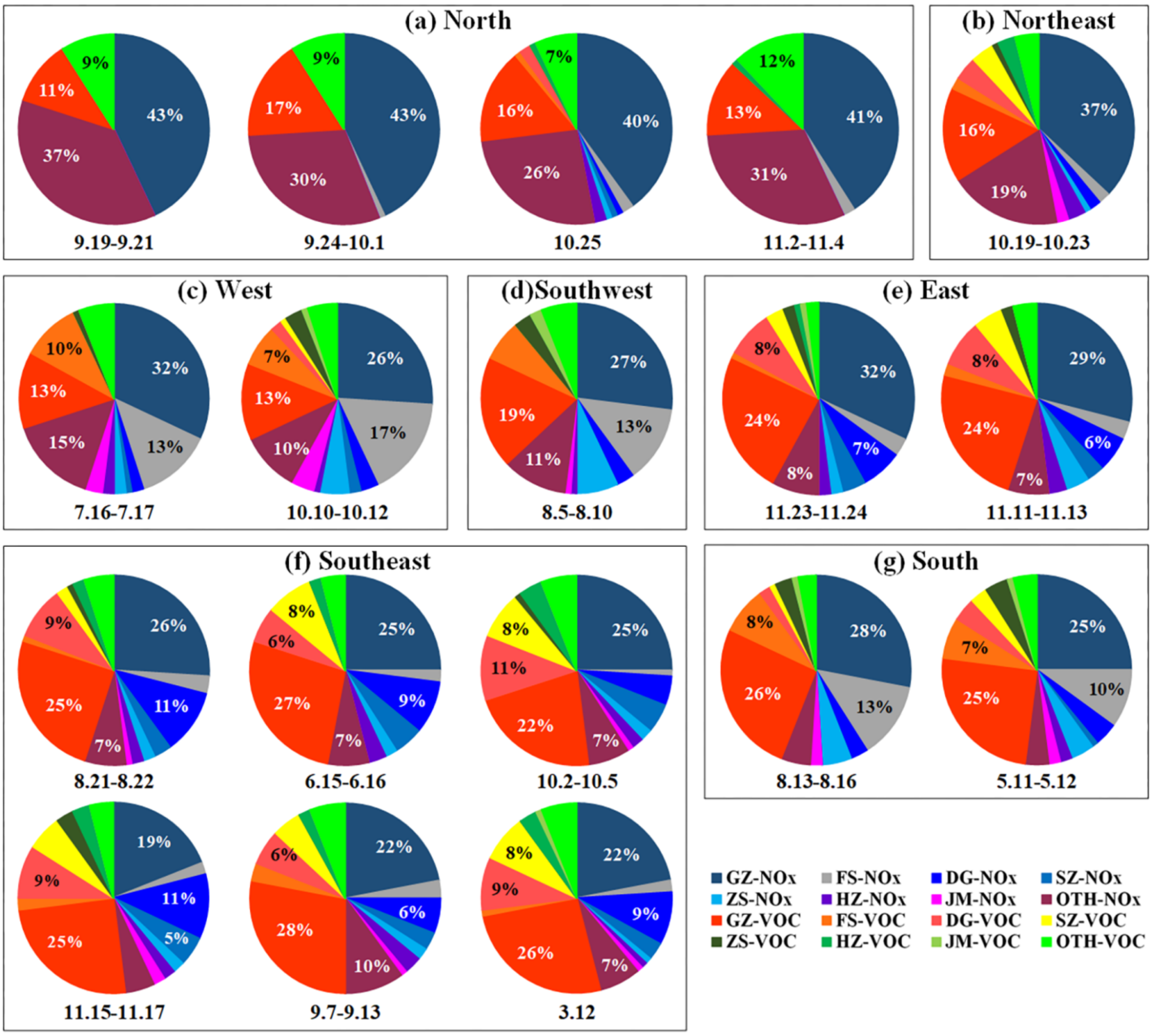

Fig. 5. The anthropogenic NO_x and VOC emission contributions from each source region in the d03 domain to O_3 of GZ under various prevailing wind directions.

Table 1. Synoptic patterns and their corresponding meteorological characteristics in O_3 polluted days of GZ 2019.

Type (Season of occurrence)	**Total days**	**The average value of MDA8 O_3 concentration (Range)^a**	**Mean temperature (Range)^b**	**Mean relative humidity (Range)^c**	**Mean wind speed (Range)^d**	**Prevailing wind direction**
Cyclone (Summer, Autumn)	26	200 (165-248)	31 (20-38)	52 (24-86)	1.34 (0.4-5.3)	West/ Southwest /South/ Southeast /North/ Northeast
Anticyclone (Spring, Summer, Autumn)	14	187 (163-228)	27 (17-34)	48 (25-76)	1.32 (0.5-3.5)	South/ Southeast/ North/East
Trough (Autumn)	9	190 (163-231)	29 (18-36)	54 (30-80)	1.25 (0.1-4.6)	Southeast/ North/ East
High pressure approaching to sea (Spring, Autumn)	5	192 (165-233)	26 (20-34)	51 (22-72)	1.08 (0.3-2.4)	South/ Southeast/ East

Unit: ^{a} μg/m^3; ^{b} °C; ^{c} %; ^{d} m/s.